

# LEDiT: Your Length-Extrapolatable Diffusion Transformer without Positional Encoding

Shen Zhang<sup>\*1</sup> Yaning Tan<sup>\*2</sup> Siyuan Liang<sup>\*1</sup> Zhaowei Chen<sup>1</sup> Linze Li<sup>1</sup> Ge Wu<sup>3</sup>  
Yuhao Chen<sup>1</sup> Shuheng Li<sup>1</sup> Zhenyu Zhao<sup>1</sup> Caihua Chen<sup>2</sup> Jiajun Liang<sup>†1</sup> Yao Tang<sup>†1</sup>



Figure 1. Selected arbitrary-resolution samples ( $512^2$ ,  $512 \times 256$ ,  $256 \times 512$ ,  $384^2$ ,  $256^2$ ,  $128^2$ ). Generated from LEDiT-XL/2 trained on ImageNet  $256 \times 256$  resolution with CFG = 4.0. LEDiT can generate high-quality images with fine details beyond the training resolution.

## Abstract

Diffusion transformers (DiTs) struggle to generate images at resolutions higher than their training resolutions. The primary obstacle is that the explicit positional encodings (PE), such as RoPE, need extrapolation which degrades performance when the inference resolution differs from training. In this paper, we propose a Length-Extrapolatable Diffusion Transformer (LEDiT), a simple yet powerful architecture to overcome this limitation. LEDiT needs no explicit PEs, thereby avoiding extrapolation. The key innovations of LEDiT are intro-

ducing causal attention to implicitly impart global positional information to tokens, while enhancing locality to precisely distinguish adjacent tokens. Experiments on  $256 \times 256$  and  $512 \times 512$  ImageNet show that LEDiT can scale the inference resolution to  $512 \times 512$  and  $1024 \times 1024$ , respectively, while achieving better image quality compared to current state-of-the-art length extrapolation methods (NTK-aware, YaRN). Moreover, LEDiT achieves strong extrapolation performance with just 100K steps of fine-tuning on a pretrained DiT, demonstrating its potential for integration into existing text-to-image DiTs. Project page: <https://shenzhang2145.github.io/ledit/>

<sup>\*</sup>Equal contribution, <sup>†</sup>Corresponding author <sup>1</sup>Jiiov Technology <sup>2</sup>Nanjing University <sup>3</sup>Nankai University. Correspondence to: Shen Zhang <shen.zhang@jiiov.com>, Jiajun Liang <tracyliang18@gmail.com>, Yao Tang <tangyao@jiiov.com>.

## 1. Introduction

The architecture of diffusion models has evolved from U-Net backbones (Ronneberger et al., 2015) to transformer-based designs (Peebles & Xie, 2023; Bao et al., 2023). Diffusion Transformers (DiTs) emerge as state-of-the-art generators (Esser et al., 2024; Chen et al., 2024b). Despite their success, DiTs face critical limitations in generating images with resolutions beyond the training size (Lu et al., 2024; Wang et al., 2024a). As illustrated in Figure 2, when trained on ImageNet (Deng et al., 2009)  $256\times 256$  resolution, DiTs can generate high-quality images at the training resolution but struggle to generalize to higher resolutions such as  $512\times 512$ . Due to the expensive quadratic cost of self-attention and the limited availability of large-scale high-resolution datasets, models are typically trained at relatively small resolutions. However, real-world applications often demand higher-resolution images, posing a significant length extrapolation challenge to current DiTs.

Many studies (Press et al., 2022; Su et al., 2024; Peng et al., 2024; Kazemnejad et al., 2023; Lu et al., 2024) emphasize the role of positional encoding (PE) in length extrapolation. Rotary Positional Embeddings (RoPE) (Su et al., 2024) and several variants, such as NTK-aware scaling (bloc97, 2023) and YaRN (Peng et al., 2024) have been proposed to enhance the extrapolation of language transformers. In the vision domain, Flexible Vision Transformers (FiT) (Lu et al., 2024; Wang et al., 2024b) integrate RoPE into DiTs to adapt to varying input resolutions. Despite these advancements, performance still degrades beyond the training resolution due to the additional positions that the model has not been trained on (see Figure 2) (Ding et al., 2024). Recent studies (Haviv et al., 2022; Kazemnejad et al., 2023) challenge the need for explicit PE, showing that large language models (LLMs) without PE (NoPE) performs well in in-distribution settings and surpasses previous explicit PEs in length extrapolation. The advantage of NoPE lies in avoiding PE interpolation, which reduces performance when inference resolution differs from training. However, it remains unclear whether DiTs can similarly benefit from NoPE for resolution extrapolation. We ask: **Whether DiTs can incorporate NoPE to enhance length extrapolation abilities?**

In this paper, We propose a **Length-Extrapolatable Diffusion Transformer** (LEDiT), which removes explicit PE and can generate high-quality images at arbitrary resolutions. One essential network adjustment to length extrapolation is the adoption of causal attention. We demonstrate that causal attention can implicitly encode positional information. Specifically, we provide both theoretical and empirical evidence that token variance decreases when position increases, providing an implicit ordering (see Section 3.2). Empirical results show that the implicit positional information achieves better length extrapolation abilities than ex-

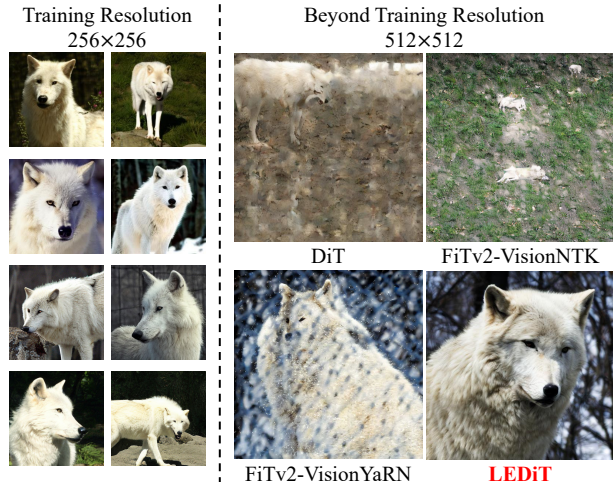


Figure 2. Diffusion Transformer performs well at the training resolution. However, when generating images beyond the training resolution, both DiT (Peebles & Xie, 2023) and FiT (Lu et al., 2024; Wang et al., 2024b) suffer significant quality degradation. In contrast, our LEDiT can generate reasonable and realistic higher-resolution images with fine-grained details. The class label is 270 (white wolf).

plicit PEs. We further introduce negligible-cost convolution with multi-dilation training strategy to enhance local fine-grained details, complementing the global coarse-grained information captured by causal attention.

We conduct extensive qualitative and quantitative experiments to validate the effectiveness of LEDiT. Specifically, LEDiT can scale the resolution to  $512\times 512$  when trained on  $256\times 256$  ImageNet, and to  $1024\times 1024$  when trained on  $512\times 512$  ImageNet, while preserving structural fidelity and fine-grained details, outperforming state-of-the-art extrapolation methods. Moreover, LEDiT can generate images with arbitrary aspect ratios (e.g.,  $512\times 384$  or  $512\times 256$ ) without employing any multiple aspect ratio training techniques. We find that fine-tuning LEDiT based on pretrained DiT weights for about 100K iterations can achieve remarkable extrapolation performance, demonstrating its potential for low-cost integration into text-to-image DiTs.

## 2. Related Work

**Diffusion Transformers.** Following the success of DiT (Peebles & Xie, 2023; Bao et al., 2023), subsequent works such as PixArt-Alpha (Chen et al., 2024b), and PixArt-Sigma (Chen et al., 2024a) extend diffusion processes with transformers for higher-quality generation. Stable Diffusion 3 (Esser et al., 2024) and Flux (Labs, 2024) have significantly enhanced the performance of diffusion transformers by scaling up parameters. Despite these advances, most DiTs struggle when inference resolution deviates from training, motivating our exploration of length

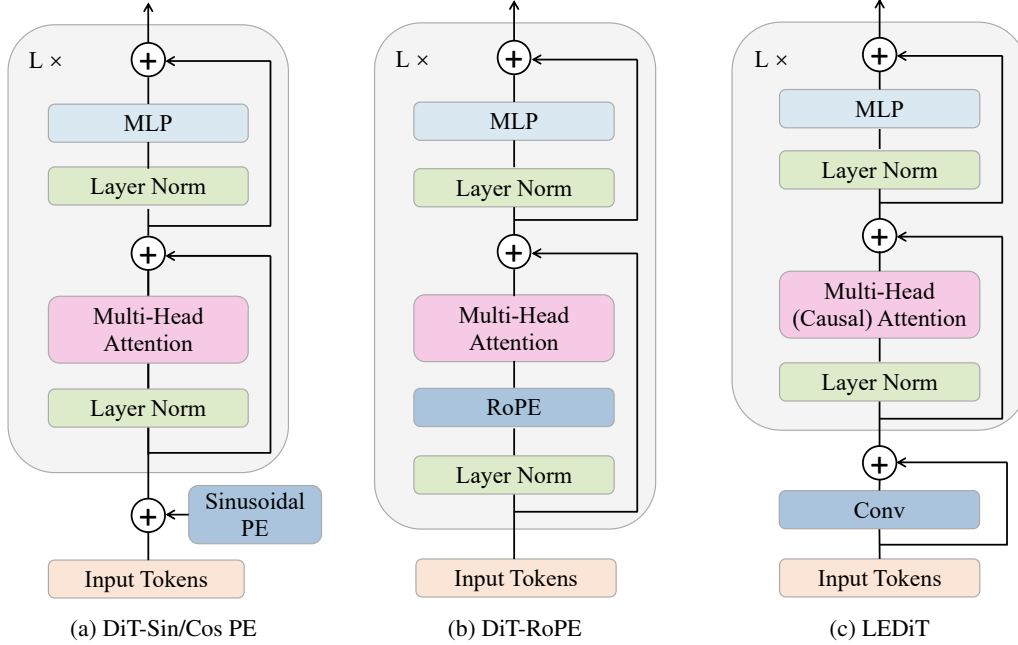


Figure 3. Comparison between DiT-Sin/Cos PE, DiT-RoPE, and our LEDiT. We omit AdaLN for the sake of simplicity. DiT-Sin/Cos PE is the vanilla DiT (Peebles & Xie, 2023), which incorporates Sinusoidal PE into the transformer. DiT-RoPE introduces rotary position encoding by rotating the query and key in each transformer block. In contrast, our LEDiT model does not require explicit position encoding. The main difference lies in the incorporation of causal attention and convolution after patchification.

extrapolation.

**Length Extrapolation in Language.** A key limitation arises from positional encodings, where traditional Absolute Positional Encoding (APE) (Vaswani et al., 2017) struggles to handle longer sequences. To address this, Rotary Position Embedding (RoPE) (Su et al., 2024) was introduced, yet its effectiveness diminishes at extreme lengths. ALiBi (Press et al., 2022) modifies attention biases to facilitate length extrapolation. Consequently, refinements such as NTK-aware adjustments (bloc97, 2023), YaRN (Peng et al., 2024), and Random Positional Encoding (RandomPE) (Ruoss et al., 2023), which broadens the sampling range, have been proposed to enhance length generalization. Meanwhile, Data-Adaptive Positional Encoding (DAPE) (Zheng et al., 2024) and Contextual Positional Encoding (CoPE) (Golovneva et al., 2024) explore adaptive embeddings. Although these methods underscore the flexible positional encodings, they mainly target language-based tasks, leaving open questions for vision-centric domains.

**Length Extrapolation in Diffusion.** Many works have explored the length extrapolation in the diffusion U-Net architecture (He et al., 2024; Zhang et al., 2024; Du et al., 2024). However, there is limited research about length extrapolation in DiTs. RoPE-Mixed (Heo et al., 2024) employs rotation-based embeddings for variable image sizes, and FiT (Lu et al., 2024; Wang et al., 2024b) adapts RoPE, NTK-Aware and YaRN to 2D variants for extrapolation.

However, existing solutions typically rely on explicit PE or only handle moderate resolution changes. A comprehensive strategy for high-resolution extrapolation in diffusion transformers remains elusive. In this work, we address this gap by enabling DiTs to generate high-fidelity images at arbitrary resolutions without explicit PE.

### 3. Method

We first introduce some preliminaries about DiTs and causal attention. DiTs is primarily built upon the ViT (Dosovitskiy et al., 2021). Each DiT block contains a multi-head self-attention (MSA), followed by adaptive layer normalization (AdaLN) and a feed-forward network (MLP). Residual connections are applied by scaling  $\alpha_\ell$  and  $\alpha'_\ell$ . Given an input  $x \in \mathbb{R}^{H \times W \times C}$ , the computation of DiT block is as follows:

$$z_0 = \text{Flatten}(\text{Patchify}(x)) + E_{\text{pos}}, \quad (1)$$

$$z'_\ell = \text{MSA}(\text{adaLN}(z_{\ell-1}, t, c)) + \alpha_\ell z_{\ell-1}, \quad (2)$$

$$z_\ell = \text{MLP}(\text{adaLN}(z'_\ell, t, c)) + \alpha'_\ell z'_\ell. \quad (3)$$

Causal attention only allows the given position in a sequence to attend to the previous positions, not to future positions. The causal attention map is:

$$A = \text{softmax} \left( \frac{QK^\top}{\sqrt{d_k}} + M \right), \quad (4)$$

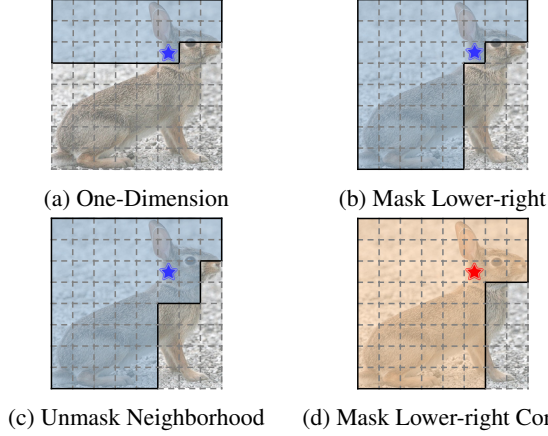


Figure 4. Comparison of causal attention scan variants. We use variant (d) as our default.

where  $Q \in \mathbb{R}^{n \times d_k}$  and  $K \in \mathbb{R}^{n \times d_k}$  are query and key,  $d_k$  is the dimension, and  $M \in \mathbb{R}^{n \times n}$  is a mask matrix with definition as follows:

$$M_{i,j} = \begin{cases} 0 & \text{if } j \leq i, \\ -\infty & \text{if } j > i. \end{cases} \quad (5)$$

This ensures attention scores for future tokens are nearly zero after softmax, enforcing strict causality.

### 3.1. LEDiT Block

The overall architecture of LEDiT is present in Figure 3c. Our LEDiT needs no explicit PE. Instead, we adopt causal attention and a negligible-cost convolution to implicitly capture the positional information, which shows better extrapolation performance verified in experiments. We design LEDiT blocks to alternate between causal attention and self-attention. The first LEDiT block uses self-attention, which can be written as:

$$z'_\ell = \text{MSA}(\text{adaLN}(z_{\ell-1}, t, c)) + \alpha_\ell z_{\ell-1}, \quad (6)$$

$$z_\ell = \text{MLP}(\text{adaLN}(z'_\ell, t, c)) + \alpha'_\ell z'_\ell. \quad (7)$$

The subsequent LEDiT block uses causal attention, which can be written as:

$$z'_{\ell+1} = \text{MCA}(\text{adaLN}(z_\ell, t, c)) + \alpha_{\ell+1} z_\ell, \quad (8)$$

$$z_{\ell+1} = \text{MLP}(\text{adaLN}(z'_{\ell+1}, t, c)) + \alpha'_{\ell+1} z'_{\ell+1}, \quad (9)$$

where MCA represents multi-head causal attention. We explore more LEDiT block designs in Table 1d.

### 3.2. Why Causal Attention

We integrate causal attention because it is not order-invariant, meaning that changes in input token positions lead to different outputs. Prior studies (Kazemnejad et al., 2023;

Zheng et al., 2024) suggest that causal attention can learn positional information without PE but lack a clear explanation of how this occurs. In this paper, we formally establish that, under specific assumptions, the variance of causal attention outputs encodes positional information. Specifically, we prove the following theorem:

**Theorem 3.1.** *For a Transformer architecture with Causal Attention, assume that the value  $V$  are i.i.d. with mean  $\mu_V$  and variance  $\sigma_V^2$ . Then, the variance of the causal attention output  $Y_{il}$  at position  $i$  and dimension  $l$  is approximately given by:*

$$\text{Var}(Y_{il}) \approx \frac{C}{1+i},$$

where the constant  $C = 2\sigma_V^2 + \mu_V^2$ .

Please refer to Appendix A for the complete proof of Theorem 3.1. This theorem reveals that, if the conditions are met, the variance is inversely proportional to the position  $i$  at a rate of  $\frac{1}{i+1}$ . We further conduct experiments to verify whether applying causal attention in DiT can assign different variances to different positions.

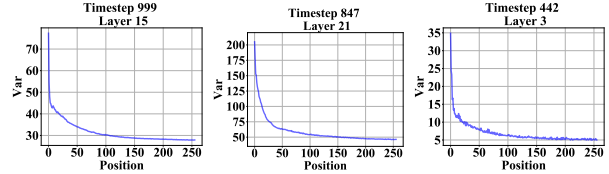


Figure 5.  $\text{Var}(y_{il})$  distributions across various timestep and DiT layers. Best viewed when zoomed in.

We train a DiT-XL/2 that replaces all self-attention with causal attention and use it to verify the theorem. Given an input sequence  $z \in \mathbb{R}^{n \times d_k}$ , causal attention takes  $z$  and outputs  $y = (y_1, \dots, y_n) \in \mathbb{R}^{n \times d_k}$ . Since each  $y_{il} \in y_i$  is derived from Gaussian noise through the same network, we assume that  $y_{i1}, \dots, y_{id_k}$  follow the same distribution. Therefore, we approximate  $\text{Var}(y_{il})$  using the variance of  $y_i$ . As shown in Figure 5,  $\text{Var}(y_{il})$  is inversely proportional to the position  $i$  across various timestep and layers. This indicates the existence of causal attention in DiT that meets the conditions of the theorem. Intuitively, a smaller  $\text{Var}(y_i)$  indicates that its elements are more concentrated. During training, the network can learn to determine the token position based on the concentration of  $y_i$ , thereby implicitly encoding positional information. We also observe variance distribution that differs from the theorem, see the appendix for more discussion.

In addition to providing implicit positional information to tokens, causal attention also acts as a learnable and global module, which differs from static positional encodings. It can make predictions based on previous token information and learn the dependencies between tokens from large-scale

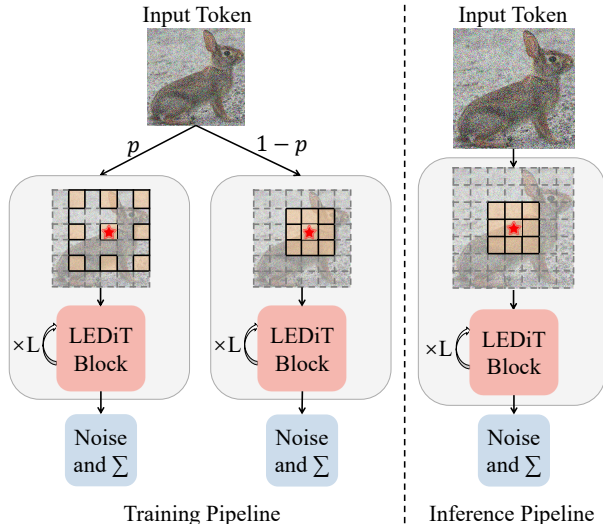


Figure 6. Training and inference pipeline of LEDiT.

data. This characteristic can enhance the model’s ability to extrapolate to higher resolution.

**Causal scan variants.** We introduce four causal attention scan variants, as depicted in Figure 4 (a) represents the traditional 1D scan used in PixelCNN (Van den Oord et al., 2016), where each position attends only to preceding tokens in a flattened sequence. To leverage the spatial characteristics of images, we also consider scanning along both the height and width dimensions and propose (b)–(d). We ablate the performance of these variants in Table 1b. Variant d is set as our default.

### 3.3. Locality Enhancement

Although causal attention provides tokens with global implicit positional information, when  $i$  is large, the variance between adjacent tokens becomes indistinguishable (see Figure 5), preventing accurate position information and leading to blurry images, see Figure 7. To distinguish the relative relationships between neighborhood tokens, we need to enhance the local perception abilities of the network. Specifically, we introduce convolution to enhance the locality of LEDiT. Previous work (Wu et al., 2021) replaced the qkv-projector with convolution or integrated convolution into the MLP (Xie et al., 2021) in each transformer block, which significantly increased the model’s computational cost. We find that adding a convolution after patchification is sufficient, while only increasing ignorable overhead. This can be written by slightly modifying Equation (1):

$$z_0 = \text{Flatten}(C_{3,1,1,1}(\text{Patchify}(x))), \quad (10)$$

where  $C_{k,p,s,d}$  denotes a convolution filter with kernel size  $k$ , padding  $p$ , stride  $s$ , and dilation  $d$ . Zero padding is applied, which enables convolution to leak local positional information (Islam et al., 2020; Xie et al., 2021).

**Multi-dilation training strategy.** Although the generated higher-resolution images are visually compelling, they often encounter duplicated object artifacts due to the fixed receptive fields of convolutional kernels (He et al., 2024). To mitigate this problem, we adopt a multi-dilation training strategy, wherein dilation and padding are randomly adjusted during training (see Figure 6). For a standard convolution filter  $C_{3,1,1,1}$ , we set a probability  $p$  to expand both its dilation rate and padding size to 2, transforming it into  $C_{3,2,1,2}$ . During inference, we empirically find that fix dilation and padding as 1 is sufficient. This strategy trains shared-parameter convolutions with varying receptive fields and empirically improves extrapolation abilities.

## 4. Experiments

### 4.1. Experiment Settings

**Model Architecture.** We follow DiT-XL (Peebles & Xie, 2023) to set the same layers, hidden size, and attention heads for XLarge model LEDiT-XL. We use a patch size  $p = 2$ , denoted by LEDiT-XL/2. LEDiT adopts the same off-the-shelf pre-trained VAE (Kingma & Welling, 2014) as DiT provided by the Stable Diffusion (Rombach et al., 2022). All experiments are conducted on LEDiT-XL/2.

**Training Details.** The experiments are conducted on the ImageNet dataset (Deng et al., 2009) with  $256 \times 256$  and  $512 \times 512$  resolutions. We train LEDiT-XL/2 (i) using random initialization or (ii) fine-tuning based on a pretrained DiT model weights to thoroughly evaluate the performance. We train the randomly initialized LEDiT for 400K steps or fine-tune LEDiT for 100K steps. We all adopt a constant learning rate of  $1 \times 10^{-4}$  using AdamW (Kingma & Ba, 2015), no weight decay and a batch size of 256. we adopt an exponential moving average (EMA) of model weights over training with a decay of 0.9999. All results are reported using the EMA model. We retain the same diffusion hyper-parameters as DiT.

**Evaluation Metrics.** We measure performance with Fréchet Inception Distance (FID) (Heusel et al., 2017), the standard metric for evaluating vision generative models. We use 250 DDPM sampling steps and report FID-50K without further elaboration. For fair comparison, all values reported in this paper are obtained by exporting samples and using ADM’s TensorFlow evaluation suite (Dhariwal & Nichol, 2021). FID reported in this section use classifier-free guidance (Ho & Salimans, 2022) scale as 1.5 (CFG=1.5). We additionally report Inception Score (Salimans et al., 2016), sFID (Nash et al., 2021) and Precision/Recall (Kynkäänniemi et al., 2019) as secondary metrics.

**Evaluation Resolution.** Compared to previous work (Lu et al., 2024; Wang et al., 2024b), this paper tests at more extreme resolutions. When trained on ImageNet

case	FID↓	IS↑
NoPE	378.95	3.79
+ Causal	286.01	6.96
+ Conv	130.91	28.66
+ Causal + Conv	<b>35.86</b>	<b>139.91</b>

(a) **Components ablations.** Causal attention and convolution are effective.

order	FID↓	IS↑
CA×L/2 + SA×L/2	36.81	139.88
SA×L/2 + CA×L/2	48.65	103.14
(CA,SA)×L/2	36.05	<b>143.26</b>
(SA,CA)×L/2	<b>35.86</b>	139.91

(d) **Block design.** The alternating order shows stable performance.

scan	FID↓	IS↑
(a)	62.49	78.25
(b)	89.77	50.10
(c)	43.17	116.03
(d)	<b>35.86</b>	<b>139.91</b>

(b) **Casual scan variants.** 2D casual scan variants outperform 1D variants.

prob	FID↓	IS↑
0	39.20	127.84
0.1	<b>35.86</b>	<b>139.91</b>
0.2	37.99	135.85
0.5	37.56	133.07

(e) **Multi-dilation probability.** LEDiT with a small probability works better.

case	FID↓	IS↑
w/o multi-dila	39.20	127.84
w/ multi-dila	<b>35.86</b>	<b>139.91</b>

(c) **Multi-dilation strategy.** LEDiT benefits from multi-dilation strategy.

dilation	FID↓	IS↑
1	39.20	127.84
2	<b>35.86</b>	<b>139.91</b>
(2,3)	37.24	136.23

(f) **Dilation rate.** (2,3) means randomly selecting 2 or 3 as the rate during training.

Table 1. Ablations using LEDiT-XL/2 on  $256\times 256$  ImageNet. We report FID and IS scores. For each ablation, we load the pretrained DiT weights and fine-tune LEDiT-XL/2 for 100K iterations. Default settings are marked in gray. See Figure 7 and Figure 10 for visualization.

$256\times 256$  resolution, we evaluate the extrapolation performance of LEDiT at  $384\times 384$  ( $2.25\times$ ),  $448\times 448$  (about  $3\times$ ), and  $512\times 512$  ( $4\times$ ) resolutions. When trained at ImageNet  $512\times 512$  resolution, we test at  $768\times 768$  ( $2.25\times$ ),  $896\times 896$  (about  $3\times$ ), and  $1024\times 1024$  ( $4\times$ ) resolutions. Additionally, we assess performance at different aspect ratios, specifically  $512\times 384$  ( $3:2$ ) and  $384\times 512$  ( $2:3$ ). All token lengths are much larger than the training token length.

**Comparison Methods.** There is limited research on length extrapolation for DiTs. The main approach (Lu et al., 2024; Wang et al., 2024b) involves applying the commonly used RoPE (Su et al., 2024) from LLMs to DiT. The RoPE extrapolation methods NTK-Aware (bloc97, 2023) and YaRN (Peng et al., 2024) are adapted for 2D extrapolation, resulting in VisionNTK (Lu et al., 2024) and VisionYaRN (Lu et al., 2024). This paper mainly compares LEDiT with VisionNTK and VisionYaRN. We apply VisionNTK and VisionYaRN to DiT and FiTv2 to evaluate existing extrapolation methods comprehensively and compare the results with LEDiT.

## 4.2. LEDiT Ablations

In this section, we ablate LEDiT design settings on  $256\times 256$  ImageNet. We use LEDiT-XL/2 to ensure that our method works at scale. We evaluate performance by loading DiT pretrained weights and fine-tuning for 100K iterations. We set CFG=1.5 and generate 10K images with  $512\times 512$  resolution and report FID-10K and IS-10K.

**Components ablations.** Table 1a shows the influence of each component of LEDiT. Removing PE (NoPE) degrades DiT severely. Both causal attention and convolution can significantly enhance extrapolation performance. Combining these two components decreases the FID from 378.95 to

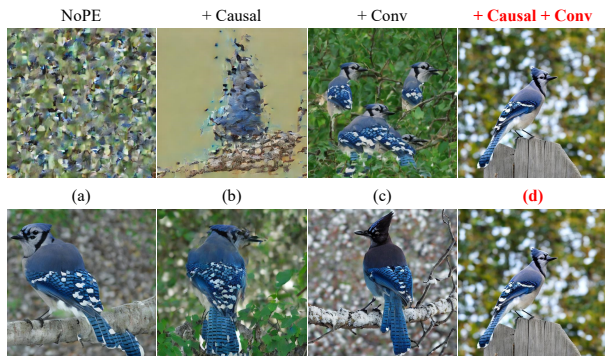


Figure 7. Visualization of the ablation study. The first row illustrates the ablations of the components proposed in this paper, while the second row displays the ablations of the causal scan variants. The models are trained on  $256\times 256$  ImageNet and generate images with  $512\times 512$  resolution. We set CFG=4.0. Best viewed when zoomed in. See Figure 10 for more visualization.

35.86 and increases IS from 3.79 to 139.91, yielding the optimal performance. Figure 7 illustrates the impact of causal attention and convolution. DiT with NoPE noise-like outputs, indicating that without PE, DiT cannot capture token positional information. Incorporating causal attention yields structurally coherent objects but insufficient high-frequency details, since causal attention provides a global ordering but struggles with local distinctions (see Section 3.3). Conversely, introducing convolution provides adequate high-frequency details, but leads to duplicated objects due to the lack of a global receptive field. When both are combined, the generated images exhibit realistic object structures as well as fine-grained details. Therefore, we use both causal attention and convolution as the default setting.

**Causal scan variants.** Table 1b presents a quantitative comparison of different scan variants. Except for variant (b), 2D scan variants (c) and (d) outperform the 1D variant (a)

Model	384×384					448×448					512×512				
	FID↓	sFID↓	IS↑	Prec.↑	Rec.↑	FID↓	sFID↓	IS↑	Prec.↑	Rec.↑	FID↓	sFID↓	IS↑	Prec.↑	Rec.↑
DiT-Sin/Cos PE*	114.10	162.50	14.91	0.18	0.27	188.42	191.58	4.19	0.06	0.11	216.22	188.69	2.70	0.10	0.04
DiT-VisionNTK*	45.81	80.42	99.92	0.48	0.42	124.88	113.88	37.79	0.22	<b>0.39</b>	174.68	139.23	16.28	0.10	0.30
DiT-VisionYaRN*	23.45	53.25	<b>138.46</b>	0.63	<b>0.35</b>	64.93	88.59	70.04	0.36	0.34	109.00	109.88	38.38	0.21	<b>0.30</b>
LEDiT*	<b>15.98</b>	<b>30.94</b>	138.25	<b>0.75</b>	0.31	<b>29.84</b>	<b>48.06</b>	<b>103.05</b>	<b>0.61</b>	0.25	<b>56.02</b>	<b>65.99</b>	<b>63.26</b>	<b>0.43</b>	0.21
DiT-Sin/Cos PE	87.03	116.67	44.93	0.31	0.31	168.23	145.45	15.25	0.12	0.23	213.77	168.51	7.98	0.06	0.13
DiT-VisionNTK	71.23	80.69	67.42	0.33	0.51	184.29	122.99	16.94	0.10	0.41	246.56	144.99	8.82	0.04	0.17
DiT-VisionYaRN	13.51	35.35	244.42	0.71	0.39	28.23	50.81	170.22	0.56	0.35	49.86	64.63	109.34	0.42	<b>0.35</b>
FiTv2-VisionNTK	38.43	47.09	107.89	0.45	<b>0.54</b>	179.01	117.12	18.20	0.08	0.42	257.63	171.10	6.72	0.01	0.21
FiTv2-VisionYaRN	23.23	35.13	157.93	0.55	0.48	71.94	64.72	64.49	0.29	<b>0.51</b>	155.80	118.21	20.76	0.11	0.27
LEDiT	<b>9.34</b>	<b>25.02</b>	<b>281.09</b>	<b>0.78</b>	0.39	<b>17.62</b>	<b>39.43</b>	<b>214.90</b>	<b>0.66</b>	0.34	<b>33.25</b>	<b>54.36</b>	<b>138.01</b>	<b>0.52</b>	0.31

Table 2. Comparison of state-of-the-art extrapolation methods and our LEDiT trained on 256×256 ImageNet at various resolutions beyond the training image size. We set CFG=1.5. \* indicates training from scratch.

Model	768×768					896×896					1024×1024				
	FID↓	sFID↓	IS↑	Prec.↑	Rec.↑	FID↓	sFID↓	IS↑	Prec.↑	Rec.↑	FID↓	sFID↓	IS↑	Prec.↑	Rec.↑
DiT-Sin/Cos PE	159.52	187.92	7.76	0.12	0.24	229.93	217.70	3.27	0.03	0.08	281.57	240.17	2.16	0.01	0.03
DiT-VisionNTK	28.94	96.37	142.35	0.67	0.53	64.41	139.97	64.52	0.48	0.47	109.31	170.58	25.31	0.29	0.39
DiT-VisionYaRN	29.46	61.37	161.32	0.66	0.53	65.58	91.48	83.21	0.50	<b>0.51</b>	104.62	118.03	43.04	0.35	<b>0.47</b>
FiTv2-VisionNTK	251.73	195.83	3.44	0.02	0.12	309.13	230.84	2.54	0.01	0.01	349.76	240.17	2.43	0.01	0.01
FiTv2-VisionYaRN	51.13	64.48	70.40	0.49	<b>0.62</b>	215.72	175.75	6.33	0.06	0.41	327.26	217.01	2.91	0.01	0.08
LEDiT	<b>21.75</b>	<b>49.81</b>	<b>176.26</b>	<b>0.71</b>	0.52	<b>48.64</b>	<b>73.25</b>	<b>97.54</b>	<b>0.56</b>	0.50	<b>91.11</b>	<b>108.70</b>	<b>48.13</b>	<b>0.40</b>	0.44

Table 3. Comparison of state-of-the-art extrapolation methods and our LEDiT trained on 512×512 ImageNet at various resolutions beyond the training image size. We set CFG=1.5.

Model	Resolution	FID↓	sFID↓	IS↑	Prec.↑	Rec.↑
DiT-Sin/Cos PE	512×384	153.74	144.66	16.52	0.13	0.27
DiT-VisionNTK		179.71	117.81	15.88	0.09	0.36
DiT-VisionYaRN		25.69	46.22	176.19	0.58	0.36
FiTv2-VisionNTK		177.44	114.56	17.14	0.08	0.40
FiTv2-VisionYaRN		56.04	51.05	81.96	0.35	<b>0.47</b>
LEDiT		<b>20.29</b>	<b>38.52</b>	<b>191.69</b>	<b>0.63</b>	0.35
DiT-Sin/Cos PE	384×512	158.21	139.80	16.98	0.14	0.26
DiT-VisionNTK		150.70	110.67	25.88	0.14	0.41
DiT-VisionYaRN		22.02	48.72	202.03	0.61	0.35
FiTv2-VisionNTK		150.70	110.67	25.88	0.14	0.41
FiTv2-VisionYaRN		49.67	57.07	99.29	0.39	<b>0.41</b>
LEDiT		<b>18.82</b>	<b>42.64</b>	<b>205.38</b>	<b>0.64</b>	0.36

Table 4. Comparison of state-of-the-art extrapolation methods and our LEDiT trained on 256×256 ImageNet at arbitrary aspect ratios. We set CFG=1.5.

in both FID and IS. Figure 7 shows that variants (c) and (d) produce more coherent object structures and finer details than variant (a). Although variant (b) is also a 2D scan, it leads to blurred images, resulting in lower FID and sFID scores. We adopt variant (d) as our default.

**Multi-dilation strategy.** By adapting to multiple receptive fields, the multi-dilation strategy enhances LEDiT’s performance and significantly mitigates object duplication. As shown in Table 1c, LEDiT with the multi-dilation strategy achieves better FID and IS scores. We adopt the multi-dilation strategy as the default setting.

**Block design.** Table 1d compares different orders of causal and self-attention blocks. The first two rows use sequential blocks, whereas the last two employ an alternating ar-

angement. Both orders achieve strong performance, but sequential order exhibits higher variance while alternating orders are more stable. We thus use the alternating order with self-attention preceding causal attention as our default.

**Multi-dilation probability.** Table 1e shows the result of different  $p$  values for multi-dilation. As  $p$  increases, FID initially decreases and then rises. When  $p = 0$ , the multi-dilation strategy is disabled, forcing the kernel to remain fixed. When  $p = 0.5$ , half of the training iterations use a  $3\times 3$  receptive field, while the other half uses a  $5\times 5$  receptive field. We find that frequent conv parameter changes during training slow convergence and introduce instability, leading to worse performance, while smaller  $p$  results in lower FID. So we adopt  $p = 0.1$  as the default setting.

**Dilation rate.** We also evaluate different dilation rates  $r$  to accommodate multiple receptive fields (Table 1f). For instance,  $r = (2, 3)$  means there is a  $p/2$  probability of choosing  $r = 2$  or  $r = 3$ . It can be seen that both  $r = 2$  and  $r = (2, 3)$  can improve performance, but  $r = (2, 3)$  is less effective than  $r = 2$ , likely due to the increased complexity of handling multiple dilation values. Nevertheless, successfully adapting convolution to multiple receptive fields may further benefit extrapolation. In this paper, we retain  $r = 1$  by default.

### 4.3. Main Results

**256×256 ImageNet.** In Figure 8, we present a qualitative comparison between LEDiT and other methods. Vanilla

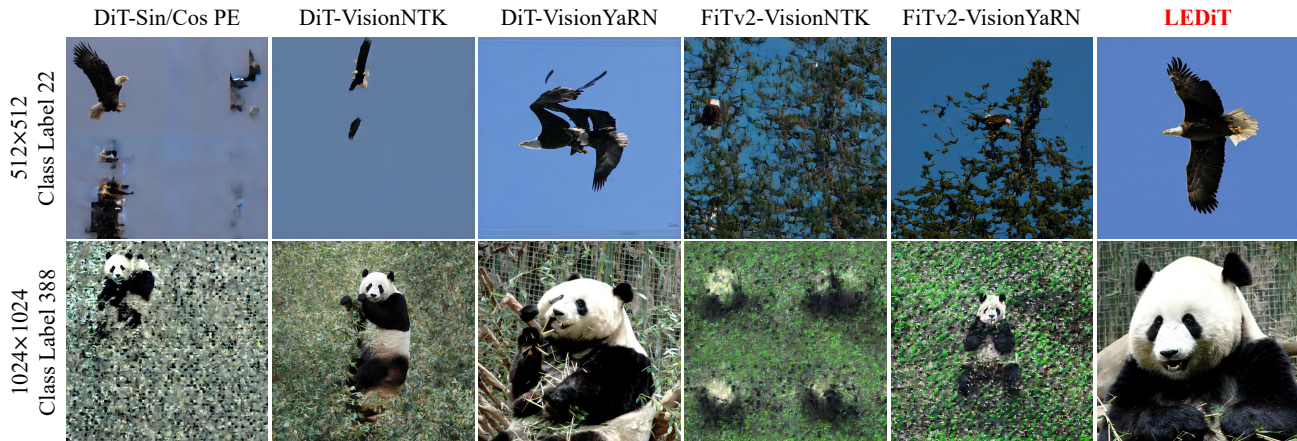


Figure 8. Qualitative comparison with other methods. The resolution and class label are located to the left of the image. We use the model trained on  $256 \times 256$  ImageNet to generate images at  $512 \times 512$  resolution, and the model trained on  $512 \times 512$  ImageNet to generate images at  $1024 \times 1024$  resolution. We set  $\text{CFG}=4.0$ . Best viewed when zoomed in. See Figure 11 and Figure 12 for more qualitative comparison.

DiT (DiT-Sin/Cos PE) suffers from severe image quality degradation. When combined with VisionNTK and VisionYaRN, DiT generates images with detailed textures but introduces unrealistic object structures. FiT produces images with severely degraded quality. In contrast, LEDiT produces images with realistic object structures and rich details. The quantitative comparison is reported in Table 2. LEDiT substantially outperforms previous extrapolation methods. At a resolution of  $384 \times 384$ , LEDiT reduces the previous best FID-50K of 13.51 (achieved by DiT-VisionYaRN) to 9.34. As the resolution increases, LEDiT further widens the performance gap, lowering the best previous score from 49.86 to 33.25 at  $512 \times 512$ . Even when trained from scratch, LEDiT achieves significantly better FID and sFID scores compared to its counterparts, demonstrating its effectiveness in both fine-tuning and training-from-scratch scenarios.

**$512 \times 512$  ImageNet.** We fine-tune a new LEDiT-XL/2 model on  $512 \times 512$  ImageNet for 100K iterations using the same hyperparameters as the  $256 \times 256$  model. The qualitative comparison among vanilla DiT, VisionNTK, VisionYaRN, and LEDiT is shown in Figure 8. As resolution increases from  $512 \times 512$  to  $1024 \times 1024$ , vanilla DiT exhibits further quality degradation, with significant noise artifacts. FiTv2-VisionNTK generates images with duplicated objects, while FiTv2-VisionYaRN produces blurry images with severe high-frequency detail loss. DiT-VisionNTK and VisionYaRN generate higher-quality images but exhibit object duplication in local structures. In contrast, LEDiT maintains more realistic structures and finer details. The quantitative results are reported in Table 3. Due to the heavy quadratic computational burden, we generate 10K images for evaluation. LEDiT consistently achieves superior metric scores across all resolution settings. For instance, at a resolution of  $768 \times 768$ , LEDiT improves the previous best FID

of 28.94 (achieved by DiT-VisionNTK) to 21.75.

**Arbitrary Aspect Ratio Extension.** Beyond generating square images, we evaluate the generalization abilities of LEDiT across different aspect ratios. Unlike FiT (Lu et al., 2024; Wang et al., 2024b), we do not apply multiple aspect ratio training techniques. Instead, we directly use the LEDiT-XL/2 model trained on the center-cropped  $256 \times 256$  ImageNet dataset. This highlights the model’s inherent generalization abilities. The quantitative results, reported in Table 4, demonstrate LEDiT’s superiority. It achieves the best FID scores, with 20.29 and 18.82 at resolutions of  $512 \times 384$  and  $384 \times 512$ , respectively, significantly outperforming FiTv2 and DiT. These results confirm that LEDiT can generate high-quality images across diverse aspect ratios even without various aspect ratio training techniques.

## 5. Conclusion

In this paper, we introduce a novel Diffusion Transformer, named Length-Extrapolatable Diffusion Transformer (LEDiT). LEDiT does not require explicit positional encodings such as RoPE. Instead, it implicitly extracts positional information through causal attention and convolution. Empirically, LEDiT can generate high-quality images at  $4 \times$  the training resolution (scale resolution from  $256 \times 256$  to  $512 \times 512$  and from  $512 \times 512$  to  $1024 \times 1024$ ). Compared to previous extrapolation methods, we can generate images with more accurate object structures and richer details. Furthermore, fine-tuning LEDiT based on pretrained DiT weights for a few iterations can achieve remarkable performance, demonstrating its potential for cost-effective integration into text-to-image Diffusion Transformers.

**Limitations and future work:** We demonstrate that causal



attention can implicitly extract positional information from a variance perspective. However, as the position increases, the variance becomes indistinguishable. Further exploration is needed to improve causal attention for extracting more precise positional information. Moreover, LEDiT can be integrated into text-to-image diffusion models or LLMs to achieve more amazing outcomes.

## Impact Statement

This paper presents work whose goal is to advance the field of Machine Learning. There are many potential societal consequences of our work, none which we feel must be specifically highlighted here.

## References

- Bao, F., Nie, S., Xue, K., Cao, Y., Li, C., Su, H., and Zhu, J. All are worth words: A vit backbone for diffusion models. In *CVPR*, pp. 22669–22679, 2023.
- bloc97. Ntk-aware scaled rope allows llama models to have extended (8k+) context size without any fine-tuning and minimal perplexity degradation. [https://www.reddit.com/r/LocalLLaMA/comments/141lz7j5/ntkaware\\_scaled\\_rope\\_allows\\_llama\\_models\\_to\\_have/](https://www.reddit.com/r/LocalLLaMA/comments/141lz7j5/ntkaware_scaled_rope_allows_llama_models_to_have/), 2023.
- Chen, J., Ge, C., Xie, E., Wu, Y., Yao, L., Ren, X., Wang, Z., Luo, P., Lu, H., and Li, Z. Pixart- $\sigma$ : Weak-to-strong training of diffusion transformer for 4k text-to-image generation. In *ECCV*, pp. 74–91. Springer, 2024a.
- Chen, J., Yu, J., Ge, C., Yao, L., Xie, E., Wu, Y., Wang, Z., Kwok, J., Luo, P., Lu, H., et al. Pixart- $\alpha$ : Fast training of diffusion transformer for photorealistic text-to-image synthesis. In *ICLR*, 2024b.
- Deng, J., Dong, W., Socher, R., Li, L.-J., Li, K., and Fei-Fei, L. Imagenet: A large-scale hierarchical image database. In *CVPR*, pp. 248–255, 2009.
- Dhariwal, P. and Nichol, A. Diffusion models beat gans on image synthesis. In *NeurIPS*, pp. 8780–8794, 2021.
- Ding, Y., Zhang, L. L., Zhang, C., Xu, Y., Shang, N., Xu, J., Yang, F., and Yang, M. Longrope: Extending llm context window beyond 2 million tokens. In *ICML*, 2024.
- Dosovitskiy, A., Beyer, L., Kolesnikov, A., Weissenborn, D., Zhai, X., Unterthiner, T., Dehghani, M., Minderer, M., Heigold, G., Gelly, S., et al. An image is worth 16x16 words: Transformers for image recognition at scale. In *ICLR*, 2021.
- Du, R., Chang, D., Hospedales, T., Song, Y.-Z., and Ma, Z. Demofusion: Democratising high-resolution image generation with no \$\$\$\$. In *CVPR*, pp. 6159–6168, 2024.
- Esser, P., Kulal, S., Blattmann, A., Entezari, R., Müller, J., Saini, H., Levi, Y., Lorenz, D., Sauer, A., Boesel, F., et al. Scaling rectified flow transformers for high-resolution image synthesis. In *ICML*, 2024.
- Golovneva, O., Wang, T., Weston, J., and Sukhbaatar, S. Contextual position encoding: Learning to count what’s important. *arXiv preprint arXiv:2405.18719*, 2024.
- Haviv, A., Ram, O., Press, O., Izsak, P., and Levy, O. Transformer language models without positional encodings still learn positional information. In *EMNLP*, 2022.
- He, Y., Yang, S., Chen, H., Cun, X., Xia, M., Zhang, Y., Wang, X., He, R., Chen, Q., and Shan, Y. Scalecrafter: Tuning-free higher-resolution visual generation with diffusion models. In *ICLR*, 2024.
- Heo, B., Park, S., Han, D., and Yun, S. Rotary position embedding for vision transformer. In *ECCV*, pp. 289–305. Springer, 2024.
- Heusel, M., Ramsauer, H., Unterthiner, T., Nessler, B., and Hochreiter, S. Gans trained by a two time-scale update rule converge to a local nash equilibrium. In *NeurIPS*, 2017.
- Ho, J. and Salimans, T. Classifier-free diffusion guidance. *arXiv preprint arXiv:2207.12598*, 2022.
- Islam, M. A., Jia, S., and Bruce, N. D. How much position information do convolutional neural networks encode? In *ICLR*, 2020.
- Kazemnejad, A., Padhi, I., Natesan Ramamurthy, K., Das, P., and Reddy, S. The impact of positional encoding on length generalization in transformers. In *NeurIPS*, 2023.
- Kingma, D. and Ba, J. Adam: A method for stochastic optimization. In *ICLR*, 2015.
- Kingma, D. P. and Welling, M. Auto-encoding variational bayes. In *ICLR*, 2014.
- Kynkäänniemi, T., Karras, T., Laine, S., Lehtinen, J., and Aila, T. Improved precision and recall metric for assessing generative models. In *NeurIPS*, 2019.
- Labs, B. F. Flux: Efficient latent space modeling for image generation. <https://github.com/black-forest-labs/flux>, 2024.
- Lu, Z., Wang, Z., Huang, D., Wu, C., Liu, X., Ouyang, W., and Bai, L. Fit: Flexible vision transformer for diffusion model. In *ICML*, 2024.
- Nash, C., Menick, J., Dieleman, S., and Battaglia, P. Generating images with sparse representations. In *ICML*, pp. 7958–7968. PMLR, 2021.

- Peebles, W. and Xie, S. Scalable diffusion models with transformers. In *ICCV*, pp. 4195–4205, 2023.
- Peng, B., Quesnelle, J., Fan, H., and Shippole, E. Yarn: Efficient context window extension of large language models. In *ICLR*, 2024.
- Press, O., Smith, N. A., and Lewis, M. Train short, test long: Attention with linear biases enables input length extrapolation. In *ICLR*, 2022.
- Rombach, R., Blattmann, A., Lorenz, D., Esser, P., and Ommer, B. High-resolution image synthesis with latent diffusion models. In *CVPR*, pp. 10684–10695, 2022.
- Ronneberger, O., Fischer, P., and Brox, T. U-net: Convolutional networks for biomedical image segmentation. In *MICCAI*, pp. 234–241. Springer, 2015.
- Ruoss, A., Delétang, G., Genewein, T., Grau-Moya, J., Csordás, R., Bennani, M., Legg, S., and Veness, J. Randomized positional encodings boost length generalization of transformers. *Proceedings of the 61st Annual Meeting of the Association for Computational Linguistics (Volume 2: Short Papers)*, pp. 1889–1903, 2023.
- Salimans, T., Goodfellow, I., Zaremba, W., Cheung, V., Radford, A., and Chen, X. Improved techniques for training gans. In *NeurIPS*, 2016.
- Su, J., Ahmed, M., Lu, Y., Pan, S., Bo, W., and Liu, Y. Roformer: Enhanced transformer with rotary position embedding. *Neurocomputing*, 568:127063, 2024.
- Van den Oord, A., Kalchbrenner, N., Espeholt, L., Vinyals, O., Graves, A., et al. Conditional image generation with pixelcnn decoders. In *NeurIPS*, 2016.
- Vaswani, A., Shazeer, N., Parmar, N., Uszkoreit, J., Jones, L., Gomez, A. N., Kaiser, Ł., and Polosukhin, I. Attention is all you need. In *NeurIPS*, 2017.
- Wang, S., Li, Z., Song, T., Li, X., Ge, T., Zheng, B., and Wang, L. Exploring dcn-like architecture for fast image generation with arbitrary resolution. In *NeurIPS*, 2024a.
- Wang, Z., Lu, Z., Huang, D., Zhou, C., Ouyang, W., et al. Fity2: Scalable and improved flexible vision transformer for diffusion model. *arXiv preprint arXiv:2410.13925*, 2024b.
- Wu, H., Xiao, B., Codella, N., Liu, M., Dai, X., Yuan, L., and Zhang, L. Cvt: Introducing convolutions to vision transformers. In *ICCV*, pp. 22–31, 2021.
- Xie, E., Wang, W., Yu, Z., Anandkumar, A., Alvarez, J. M., and Luo, P. Segformer: Simple and efficient design for semantic segmentation with transformers. In *NeurIPS*, pp. 12077–12090, 2021.
- Zhang, S., Chen, Z., Zhao, Z., Chen, Y., Tang, Y., and Liang, J. Hidiffusion: Unlocking higher-resolution creativity and efficiency in pretrained diffusion models. In *ECCV*, pp. 145–161. Springer, 2024.
- Zheng, C., Gao, Y., Shi, H., Huang, M., Li, J., Xiong, J., Ren, X., Ng, M., Jiang, X., Li, Z., et al. Dape: Data-adaptive positional encoding for length extrapolation. In *NeurIPS*, 2024.

## A. Proofs

### Variance of Attention Output in Causal Attention

**Assumptions.** In Theorem 3.1, we demonstrate that Causal Attention introduces a position-dependent variance in attention outputs, allowing the Transformer to encode positional information implicitly.

To facilitate the subsequent derivations, we introduce the following assumptions:

- **Attention Score Distribution:** We assume that the attention scores

$$S = \frac{QK^\top}{\sqrt{d_k}} \quad (11)$$

are independently and identically distributed (i.i.d.). Specifically, the elements  $\{S_{ij}\}$  are assumed to be i.i.d., where

$$S_{ij} = \frac{1}{\sqrt{d_k}} \sum_{m=1}^{d_k} Q_{im} K_{jm}. \quad (12)$$

- **Value Distribution:** The value  $V$  is assumed to be i.i.d. with  $E[V] = \mu_V$  and  $\text{Var}(V) = \sigma_V^2$ .
- **Mutual Independence:** We assume that the attention scores  $\{S_{ij}\}$  and the value  $V$  are mutually independent.

These assumptions serve as the foundation for the subsequent theoretical analysis.

### Proof of Theorem 3.1

*Proof.* Consider a sequence of length  $n$ . For  $1 \leq i, j \leq n$ , the *causal attention matrix*  $A_{ij}$  is defined by

$$A_{ij} = \begin{cases} \frac{\exp(S_{ij})}{\sum_{j'=1}^i \exp(S_{ij'})}, & i \geq j, \\ 0, & i < j. \end{cases} \quad (13)$$

Let  $Z_{ij} = \exp(S_{ij})$  and  $W_{ij} = \frac{Z_{ij}}{\sum_{j'=1}^i Z_{ij'}}$ . Then the attention output at position  $i$  in dimension  $l$  is  $Y_{il} = \sum_{j=1}^i W_{ij} V_{jl}$ .

The variance of  $(Y_{il})$  is :

$$\text{Var}(Y_{il}) = \text{Var}\left(\sum_{j=1}^i W_{ij} V_{jl}\right) = \sum_{j=1}^i \text{Var}(W_{ij} V_{jl}), \quad (14)$$

since  $W_{ij}$  and  $V_{jl}$  are independent for each  $i, j, l$ . Furthermore,  $\text{Var}(W_{ij} V_{jl}) = E[W_{ij}^2] \sigma_V^2 + \mu_V^2 \text{Var}(W_{ij})$ . Hence,

$$\text{Var}(Y_{il}) = \sum_{j=1}^i (E[W_{ij}^2] \sigma_V^2 + \mu_V^2 \text{Var}(W_{ij})). \quad (15)$$

Because  $Z_{ij}$  are i.i.d. and positive, we have  $\sum_{j=1}^i W_{ij} = \frac{\sum_{j=1}^i Z_{ij}}{\sum_{j'=1}^i Z_{ij'}} = 1$ , hence  $E[W_{ij}] = 1/i$ .

Besides, the normalized vector  $(W_{i1}, W_{i2}, \dots, W_{ii}) = \left( \frac{Z_{i1}}{\sum_{j'=1}^i Z_{ij'}}, \dots, \frac{Z_{ii}}{\sum_{j'=1}^i Z_{ij'}} \right)$  can be approximated by a Dirichlet $(1, \dots, 1)$  distribution, because the vector obtained by normalizing several positive, identically (or approximately identically) distributed random variables can often be approximated by the Dirichlet distribution. Reasonably, whenever the exponentials  $\{\exp(S_{ij})\}$  do not differ too sharply and remain roughly exchangeable, this leads to the uniform-symmetric Dirichlet scenario. In practice, it provides a convenient closed-form  $E[W_{ij}^2] = \frac{2}{i(i+1)}$ .

Then  $\text{Var}(W_{ij}) = E[W_{ij}^2] - (E[W_{ij}])^2 = \frac{2}{i(i+1)} - \frac{1}{i^2}$ . Substituting into the sum, one obtains

$$\text{Var}(Y_{il}) = \sum_{j=1}^i \left( \frac{2}{i(i+1)} \sigma_V^2 + \mu_V^2 \left[ \frac{2}{i(i+1)} - \frac{1}{i^2} \right] \right) = \frac{2}{i+1} \sigma_V^2 + \frac{i-1}{i(i+1)} \mu_V^2. \quad (16)$$

As  $i$  increases, we can approximate  $\frac{i-1}{i(i+1)} \approx \frac{1}{i+1}$ , leading to the reasonable approximation

$$\text{Var}(Y_{il}) \approx \frac{C}{i+1}, \quad (17)$$

where the constant  $C = 2\sigma_V^2 + \mu_V^2$ .

□

## B. More Variance Distribution Visualization

As shown in Figure 9, we present the variance distribution of causal attention outputs across different timesteps and layers. During the early stages of denoising, the variance distribution mainly follows our proposed theorem. However, as denoising progresses, the variance distribution deviates from the theorem and becomes irregular. We attribute this to the higher independence among values  $V$  in the early stages, which aligns with the theorem’s assumptions. In the later stages, the increasing correlation between tokens (position and semantic relationships) violates the assumptions, which warrant further research.

## C. In-distribution Comparison

In the main text, we compared the results of various methods at resolutions higher than the training resolution. In this section, we compare performance at the training resolution to demonstrate that LEDiT does not sacrifice performance in in-distribution scenarios. As shown in Table 5, our LEDiT achieved performance comparable to DiT with explicit PE in the in-distribution scenario.

Model	Resolution	FID↓	sFID↓	IS↑	Prec.↑	Rec.↑
DiT-Sin/Cos PE		2.27	4.60	278.24	0.83	0.57
DiT-RoPE	256×256	2.33	4.65	272.02	0.82	0.57
LEDiT		2.39	4.69	263.09	0.83	0.56

Table 5. Comparison of performance on 256×256 resolution. The models are trained on 256×256 ImageNet. We set CFG=1.5.

## D. More Ablation Visualization

We present all visualizations of the ablation study in Figure 10.

## E. More Qualitative Visualization

We present more comparison results with DiT-Sin/Cos PE, DiT-VisionNTK, DiT-VisionYaRN, FiTv2-VisionNTK, and FiTv2-VisionYaRN to demonstrate the effectiveness of LEDiT, as shown in Figure 11 and Figure 12. LEDiT outperforms other methods in both fidelity and local details.

## F. Additional Samples

We present more samples generated by LEDiT-XL/2 in Figure 13 and Figure 14.

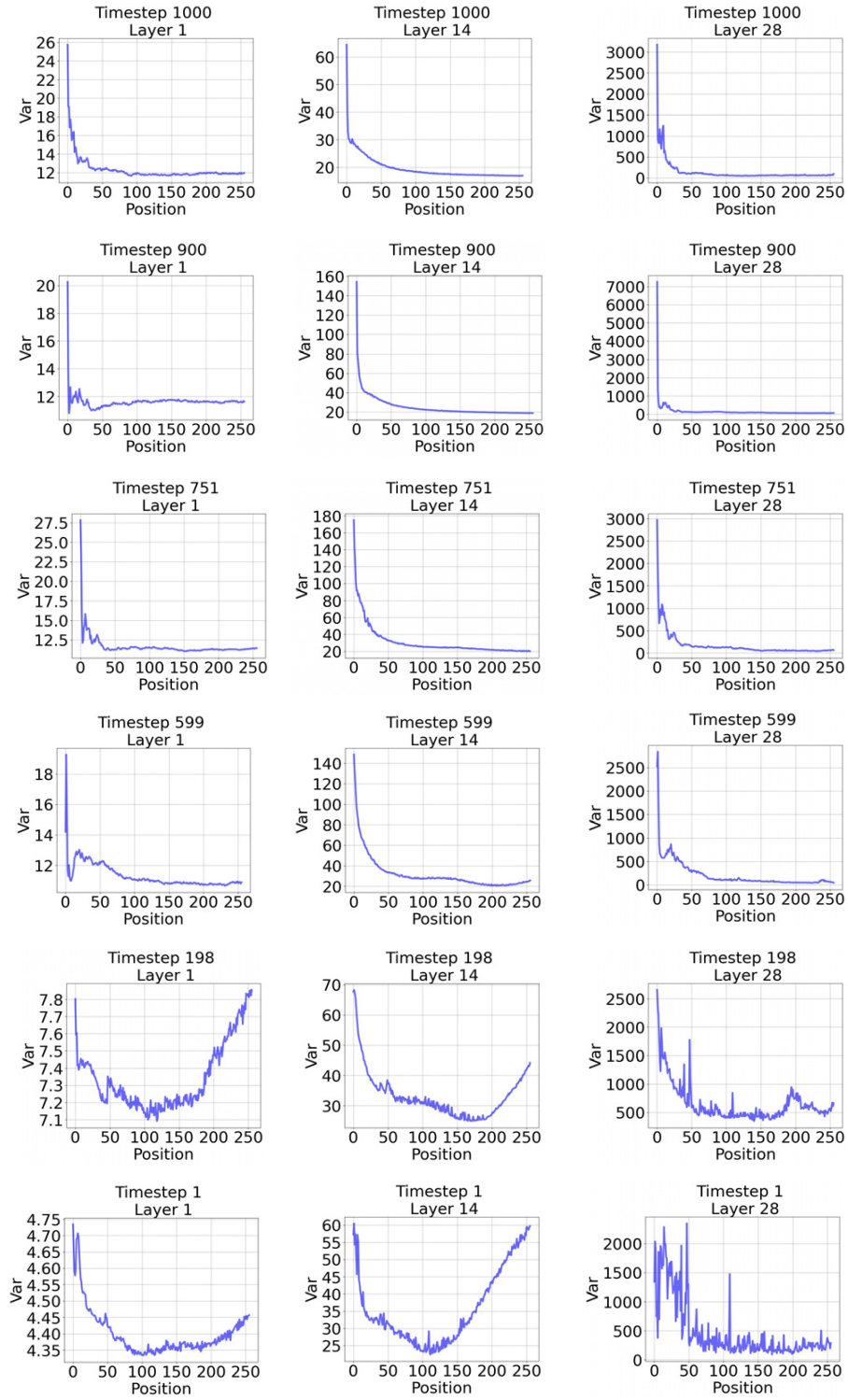


Figure 9. Variance distribution across different timesteps and layers.

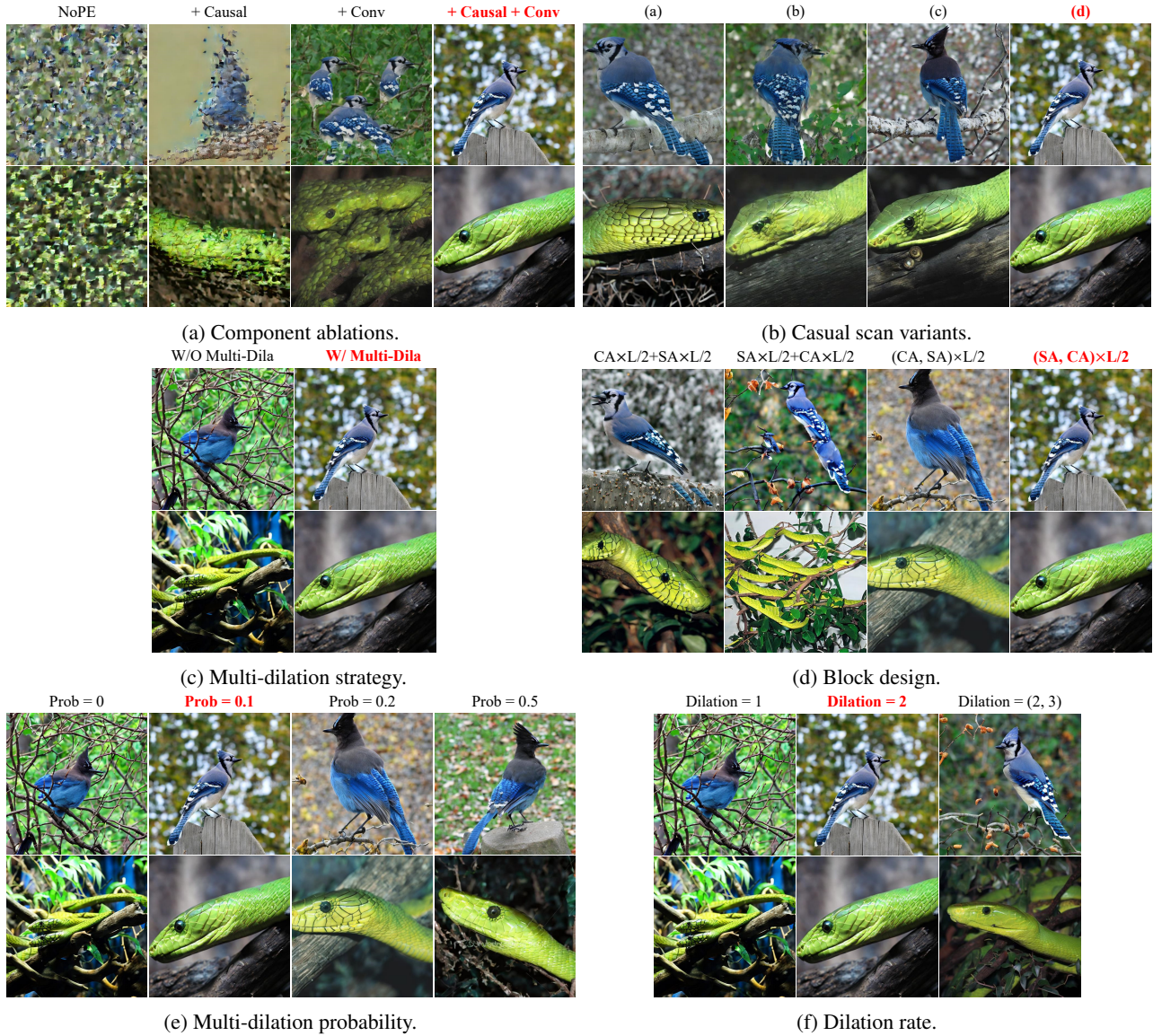


Figure 10. Ablation visualization of Table 1. We set CFG=4.0. Best viewed when zoomed in.



Figure 11. More qualitative comparison with other methods. The resolution and class label are located to the left of the image. We use the model trained on  $256 \times 256$  ImageNet to generate images with resolutions less than or equal to  $512 \times 512$ , and the model trained on  $512 \times 512$  ImageNet to generate images with resolutions greater than  $512 \times 512$  and less than or equal to  $1024 \times 1024$ . We set CFG=4.0. Best viewed when zoomed in.



Figure 12. More qualitative comparison with other methods on generating non-square images. The resolution and class label are located to the left of the image. We use the model trained on  $256 \times 256$  ImageNet to generate images at  $512 \times 384$  and  $384 \times 512$  resolutions. We set  $CFG=4.0$ . Best viewed when zoomed in.



Figure 13. More arbitrary-resolution samples ( $512^2$ ,  $512 \times 384$ ,  $384 \times 512$ ,  $384^2$ ). Generated from our LEDiT-XL/2 trained on ImageNet  $256 \times 256$  resolution. We set  $CFG = 4.0$ .





Figure 14. More arbitrary-resolution samples ( $1024^2$ ,  $1024 \times 768$ ,  $768 \times 1024$ ,  $768^2$ ). Generated from our LEDiT-XL/2 trained on ImageNet  $512 \times 512$  resolution. We set CFG = 4.0.